Thermal Pattern Contrast Diagnostic of Microcracks With Induction Thermography for Aircraft Braking Components

Yizhe Wang, *Student Member, IEEE*, Bin Gao, *Senior Member, IEEE*, Wai lok Woo, *Senior Member, IEEE*, Guiyun Tian, *Senior Member, IEEE*, Xavier Maldague, *Senior Member, IEEE*, Li Zheng, Zheyou Guo, and Yuyu Zhu

***Abstract*—Reciprocating impact load leads to plastic deformation on the surface of the kinematic chains in an aircraft brake system. As a result, this causes fatigue and various complex natural damages. Due to the complex surface conditions and the coexistence damages, it is extremely difficult to diagnose microcracks by using conventional thermography inspection methods. In this paper, the thermal pattern contrast method is proposed for weak thermal signal detection using eddy current pulsed thermography. In this process, the extraction and subsequent separation differentiate a maximum of the thermal spatial-transient pattern between defect and nondefect areas. Specifically, a successive optical flow is established to conduct a projection of the thermal diffusion. This directly gains the benefits of capturing the thermal propagation characteristics. It enables us to build the motion context connected between the local and the global thermal spatial pattern. Principal component analysis is constructed to further mine the spatial-transient patterns to enhance the detectability and sensitivity in microcrack detection. Finally, experimental studies have been conducted on an artificial crack in a steel sample and on natural fatigue cracks in aircraft brake components in order to validate the proposed method.**

Manuscript received November 7, 2017; revised January 16, 2018; accepted January 29, 2018. Date of publication February 5, 2018; date of current version December 3, 2018. The work was supported in part by the National Natural Science Foundation of China under Grant 61401071 and Grant 61527803, in part by NSAF under Grant U1430115, and in part by Engineering and Physical Sciences Research Council Impact Acceleration Account Phase 2 funded project: "3D superfast and portable eddy current pulsed thermography for railway inspection" (EP/K503885/1). Paper no. TII-17-2611. *(Corresponding author: Bin Gao.)*

Y. Wang and B. Gao are with the University of Electronic Science and Technology of China, Chengdu 610054, China (e-mail: yizhewang@uestc.edu.cn; bin_gao@uestc.edu.cn).

W. L. Woo is with the Electrical and Electronic Engineering, Newcastle University, Newcastle upon Tyne NE2 4RY, U.K. (e-mail: lok.woo@ncl.ac.uk).

G. Tian is with the School of Automation Engineering, University of Electronic Science and Technology of China, Chengdu 610054, China (e-mail: g.y.tian@ncl.ac.uk).

X. Maldague is with the Faculte des sciences et de genie, Universite Laval, Quebec, QC G1K 7P4, Canada (e-mail: maldagx@gel.ulaval.ca).

L. Zheng, Z. Guo, and Y. Zhu are with the University of Electronic Science and Technology of China, Chengdu 610054, China (e-mail: LiZheng@uestc.edu.cn; ZheyouGuo@uestc.edu.cn; yuyuzhu@uestc.edu.cn).

Color versions of one or more of the figures in this paper are available online at http://ieeexplore.ieee.org.

Digital Object Identifier 10.1109/TII.2018.2802046

***Index Terms*—Aircraft braking system, induction thermography, optical flow (OF), principal component analysis (PCA), thermal pattern contrast (TPC), weak signal extraction.**

I. Introduction

IN THE last few decades, infrared thermography [1–3] has received vast and growing attention for diagnostics and monitoring in industry. Along with the development of thermal science, the industry has put forward higher requirements, such as in-service inspection, quantification, and online measurement with robots [4]. In-service kinematic chains frequently coexist with various types of complex natural defects due to harsh working environments, such as high temperature, stress, and reciprocating impact loads [5]. Due to the complex surface conditions and the coexistence damages, it is extremely difficult to diagnose natural cracks by using a conventional thermography inspection method.

The braking system is a functionally independent subsystem of an aircraft. During the braking process, the hydraulic oil from the brake system flows into the cylinder block and then pushes the piston, compressing the movable pieces and static pieces alternately arranged in the hub [6], [7]. The driven key is a significant component in the braking system that connects an airplane wheel to the rotating disks in synchronous rotation [7]. The rotating disks brake the aviation wheels mediated by the driven keys due to the inertia of the airplane in the braking process [8]. This process leads to reciprocating impact from the slot of rotating disks on both sides of the driven keys. The repeated impact damage is part of the fatigue that manifests as a macroscopic plastic deformation. The common failure modes of repeated impact in metals include fatigue cracks [9], particle fragmentation/wear, upsetting, surface corrosion pitting, and peeling. Microcracks are considered intolerable defects and common failure mechanisms [10], which require an early diagnosis and warning for safety and prevention purposes. Therefore, it is crucial to detect and evaluate the fatigue cracks in driven keys in order to guarantee the reliability and integrity of jet braking systems.

Advanced signal processing has been used to improve the detection accuracy and precision in the thermography nonde-

1551-3203 © 2018 IEEE. Personal use is permitted, but republication/redistribution requires IEEE permission.
See http://www.ieee.org/publications_standards/publications/rights/index.html for more information.

structive testing (NDT) [11]–[19]. This can be categorized in different groups according to the manner in which data are handled [20]. Thermal contrast-based techniques are based on the thermal mechanism. Thermographic signal reconstruction (TSR) is a sophisticated thermal contrast-based method that was proposed by Steven M. Shepard in 2001 [21]. It improves the spatial and temporal resolution of a thermogram sequence [22]. It enhances the flaw contrast and improves noise rejection qualities. The image enhancement has been conducted by subjecting the raw data upon a set of logarithmic polynomial fitting of the temperature time evolution. Matrix factorization techniques have been greatly expanded in thermography processing. Principal component analysis (PCA) has been successfully used to capture the transient-spatial thermal pattern by considering the initial sequence as either a set of images or a set of temporal profiles [23]. Signal transform methods convert the detection signal into the other domain to seek effective detection information and patterns. Fourier transform was applied to pulsed thermography. It significantly enhances the flaw contrast by using the phase map [24] and image normalization [25]. Influence of nonuniform heating and surface emissivity variation is removed by using a Fourier transformation-based image reconstruction algorithm [26]. The success of these signal processing methods has one common ingredient that bridges the gap between the physical world and mathematical modeling world. For crack detection in the thermal field, under standardized specimens, several outstanding results based on advanced signal processing have been reported [27]–[30]. Vrana *et al.* researched the mechanisms and models for crack detection with induction thermography [27]. Dudzik proposed a neural algorithm to estimate defect depth using an active thermography [28]. Peng *et al.* discussed different angled defects of rolling contact fatigue in rails [29]. Gao *et al.* focus on the quantitative assessment and error analysis for the surface cracks [30]. However, previous research rarely discusses the diagnosis of natural cracks that are concealed in kinematic chains with complex geometries. It remains a challenge to extract and distinguish the weak thermal features of natural cracks from the samples with poor surface conditions and noise interference.

Eddy current pulsed thermography (ECPT) is a multiphysics coupling NDT method that belongs to the Induction Thermography family. The main physical process of ECPT involves induced eddy currents heating and thermal diffusion [31], [32]. The combination of these two physical fields is beneficial for detecting turbulence in conductive materials by analyzing the thermal patterns. The rich transient information in the ECPT spatial-transient pattern has attracted a wide range of interest [33], [34].

In this paper, a method termed as the thermal pattern contrast (TPC) is proposed to extract and separate the thermal spatial-transient patterns to enhance resolution in order to better detect microfatigue cracks through induction thermography. TPC is based on a deep understanding of the thermal mechanism. It enables us to build the motion context connected between the local and the global thermal spatial patterns that obtains the benefits from the motion extraction context in order to characterize the thermal propagation. It provides a possibility to extract and separate the thermal spatial-transient patterns between defect and nondefect areas for weak thermal signal detection. The drawback of the TPC method is the difficulty to reflect in the depth quantification of a defect. The contributions of this paper can be summarized as follows: 1) building the relationship between inductive heating propagation and thermal-OF; 2) modeling and mining of mathematical spatial-transient thermal patterns for automated crack detection. The experiments have been designed to validate the efficacy and robustness of the proposed method. First, an abstract model is built on a steel sample containing artificial cracks. Second, simulating the thermal behavior of microcracks, which involves weak thermal signal under strong background interference. Finally, the robustness of the proposed method is demonstrated by using eight different sets of natural fatigue cracks to introduce the reciprocating impact loads of the driven keys in aircraft brake systems for quantitative defect detection.

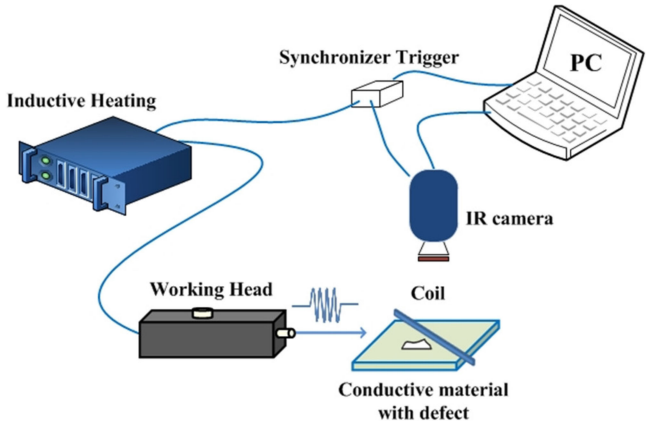

Fig. 1. ECPT schematic diagram.

The rest of this paper has been organized as follows: The theory of TPC is described in Section II. The experiments and results are analyzed and compared in Section III. Finally, conclusions and further work are outlined in Section IV.

II. Methodology of Inspection System and Image Analysis

This section serves as a basic exposition of TPC theory. First, an introduction of ECPT is presented. Then, the relationship between thermal diffusion and optical flow (OF) is derived. Data reconstruction and the principle of fixed frame-interval is then presented for thermal spatial-transient pattern extraction and separation.

A. Eddy Current Pulsed Thermography

Fig. 1 shows the schematic diagram of ECPT. The excitation signal generated by the induction heating element is a high frequency current pulse continuing during a few milliseconds. It is driven to the transmitter coil above the conductor that will induce the eddy currents and generate the resistive heat in the conductive material. Thermal diffusion leads the heat flow from a high to low-temperature area, and then reduces the contrast so as to reach a heat balance in the material. If a defect exists in the conductive material, the distribution of eddy current or the process of thermal diffusion will be disturbed. Consequently, the

resultant surface heat distribution and the transient temperature time spatial response will show the variation captured by an infrared camera.

The main physical process of ECPT consists of induced eddy currents heating and thermal diffusion. Electromagnetic governing equation can be transformed by the differential of the Maxwell equations [23], namely:

$$\nabla \times H = J + \frac{\partial D}{\partial t} = J_s + J_e + \frac{\partial D}{\partial t} \text{ (from Ampere's law)} \tag{1}$$

$$\nabla \times E = -\frac{\partial B}{\partial t} \text{ (from Faraday's law)} \tag{2}$$

where H is the magnetic field intensity, J is the total charge current density, J_s is the external current density, J_e is the induced current density, D is the electric displacement vector, E is the electric field intensity, and B is the magnetic flux density.

Constitutive equations in electromagnetism are given by

$$D = \varepsilon E \tag{3}$$

$$J_e = \sigma E \tag{4}$$

$$B = \mu H \tag{5}$$

where ε is the permittivity, σ is the electrical conductivity, and μ is the magnetic permeability of the medium. The vector potential A is defined as follows:

$$B = \nabla \times A \tag{6}$$

and assuming an axisymmetric condition, we can transform (1)–(6) into the electromagnetic governing equation:

$$\nabla \times \left(\frac{1}{\mu}\nabla \times A\right) + \sigma\frac{\partial A}{\partial t} + \varepsilon\frac{\partial^2 A}{\partial t^2} = J_s. \tag{7}$$

The excitation frequency of ECPT is typically chosen from dozens to several hundred kilohertz. At this frequency, the electric displacement vector D can be ignored in the metallic material. So (7) can be written as follows :

$$\nabla \times \left(\frac{1}{\mu}\nabla \times A\right) + \sigma\frac{\partial A}{\partial t} = J_s. \tag{8}$$

After setting the boundary conditions, the distribution of eddy currents induced in the conductor can be solved by using the finite element method through (8).

The temperature of a conducting material will increase owing to resistive heating from the induced electric current. This is known as Joule heating that is the coupling of the electromagnetic and thermal fields. The following equation expresses this relationship:

$$Q = \frac{1}{\sigma}|J_e|^2 = \frac{1}{\sigma}|\sigma E|^2. \tag{9}$$

The above equation expresses the relationship between the sum of the generated heat Q. Due to the energy conservation and Fourier heat conduction, the inductive heat conduction equation can be expressed as follows:

$$\frac{\partial T}{\partial t} = \underbrace{\frac{\lambda}{\rho C_p}\left(\frac{\partial^2 T}{\partial x^2} + \frac{\partial^2 T}{\partial y^2} + \frac{\partial^2 T}{\partial z^2}\right)}_{\text{Thermal diffusion}} + \underbrace{\frac{1}{\rho C_p}q(x,y,z,t)}_{\text{Joule heating}} \tag{10}$$

where $T = T(x, y, z, t)$ is the transient surface temperature distribution, λ is the thermal conductivity of the material (W/m K), ρ is the density (kg/m^3), C_p is the specific heat capacity (J/kg K), and $q(x, y, z, t)$ is the heat generation function per unit volume and unit time, which is the result of the Joule heating by the eddy current. The heat conduction equation is merged with Joule heating and thermal diffusion.

B. Emissivity

Infrared thermal imaging that is used to infer surface temperature from the intensity of thermal radiation is strongly dependent on surface thermal emissivity. The level of emissivity is influenced by the material, surface condition, wavelength, etc. Hence, the variations of surface emissivity on metallic surfaces involves critical challenges in the process of accurate temperature mapping and defect detection using ECPT.

To reduce the influence of emissivity variation on temperature measurement, many works have been attempted with various methods [34]–[41]. Avdelidis *et al.* [34] applied black paint on the specimen to increase the emissivity for uniform distribution and to improve the homogeneity of surface emissivity. Bai *et al.* [35] proposed a two heat-balance states based normalization to remove emissivity adverse influence of ECPT by negating the emissivity factor from the thermal radiation equation. Kasemann *et al.* [36] employed a relative emissivity distribution with its average value to correct temperature errors. Schmugge *et al.* [37] implemented temperature and emissivity separation from multispectral thermal infrared imaging using relative emissivity values. Maldague *et al.* [38] and He *et al.* [39] applied phase analysis to reduce emissivity variation influence and extracted thermal features in a specific frequency to achieve defect evaluation. Gao *et al.* [40] proposed a nonnegative matrix factorization-based thermal patterns separation model to directly identify defects and remove emissivity influence. Yunlai *et al.* [41] calculated a graphical indicator based on the normalized difference vegetation index algorithm and utilized this algorithm to reduce the influence of emissivity variation.

In this paper, we developed the preprocessing step that subtracts the first frame from the set of thermal frames for background noise reduction. This process is similar to the two heat-balance state-based normalization method [2] in which the influence of surface emissivity could be reduced on the test results. The reasons this simple method is used to reduce the emissivity and background noise are as follows:1) emphasis on the innovation of this paper. The purpose is to extract and separate the thermal spatial-transient patterns between the defect and the nondefect areas for weak thermal signal detection with maximum discrimination. 2) Prevent overtreatment in the preprocessing stage that leads to the loss of natural crack information. The challenge and motivation of this work is to detect the weak thermal signal of natural fatigue cracks under poor surface

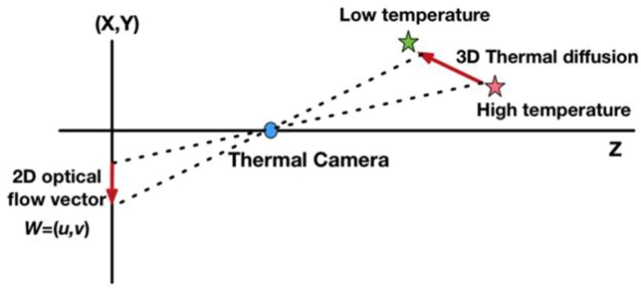

Fig. 2. Relationship between thermal diffusion and optical flow.

conditions. The goal is to detect the natural cracks that have a very low signal-to-noise ratio (SNR). The overly complicated methods may be useful in removing background noise and emissivity factor. However, the preprocessing stage will also lead to the loss of the defect information that is useful for the extraction and separation of the thermal spatial-transient pattern of TPC.

C. Thermal Transient Pattern

In the thermal field, OF indicates the projection of three-dimensional (3-D) heat propagation onto the 2-D thermal image. This is shown in Fig. 2. Each pixel (*x, y*) owns one velocity vector $w = (u, v)$ to reveal the speed of thermal diffusion at this pixel that is moving across in a certain direction $(x + u,\ y + v)$. The mathematical derivation between OF and thermal diffusion and the physical mechanism of this bonding will be introduced and explained in the following section.

In this case, the detection signal in the form of the temperature (*T*) is captured by the infrared camera. The thermal image sequence is constructed as a three-dimension spatial-transient tensor with respect to the location x and y, and time t. The intensity of each pixel (*x, y*) is defined as *T(x, y, t)*.

Based on the bright constancy assumption, the OF Constraint equation is given by

$$\frac{\partial T}{\partial x}\mu + \frac{\partial T}{\partial y}v + \frac{\partial T}{\partial t} = 0. \tag{11}$$

The OF vector is given by $w = (u, v)$, in which u and v are row vectors. The temperature gradient ∇T is expressed as $\nabla T = (T_x, T_y) = (\frac{\partial T}{\partial x}, \frac{\partial T}{\partial y})$. The time derivative $T_t = \frac{\partial T}{\partial t}$. Thus, (11) can be written as follows:

$$\nabla T \cdot w + T_t = 0. \tag{12}$$

The linearized brightness constancy constraint provides only one equation to recover the two unknown components of w. This is known as the aperture problem of the OF algorithms. Thus, the Horn–Schunck method [42] is used for the implementation, where the relationship between the OF w and the temperature gradient ∇T is formulated as a global energy function that is solved through minimization.

The above formula establishes the bridge between OF and the temperature gradient. According to Fourier's law of heat conduction [31]:

$$Q = -k \cdot \nabla T. \tag{13}$$

The thermal diffusion through a material is negatively proportional to the temperature gradient. Therefore, the OF vector displays thermal diffusion, whose direction is opposite to that of the temperature gradient, according to (12) and (13).

D. Feature Extraction and Separation

The OF characterizes the thermal behavior; however, the result of the OF solely expresses the thermal diffusion between two images that only consider spatial information of the thermal diffusion in one moment. Thus, information is lost on the development of the whole thermal transient progress. This leads to the next logical move: exploring sufficient information from the multidomain (spatial transient) for feature extraction.

The result of OF between two frames could be characterized as a two-dimensional array in which each pixel contains vector information: the direction and length of the arrows, representing the heat propagation indirectly. For data reconstitution, every two images from the original thermal image sequence (*Y*) with a fixed frame-interval in turn calculate the successive OF that will generate a new OF sequence (Y_{OF}) as the input of PCA. This successive OF image sequence can be regarded as a three-dimensional matrix. The PCA algorithm can be used for defect separation [43]. This mathematical model can be described as [33] follows:

$$Y_{\mathrm{OF}}(t) = \sum_{i=1}^{N_s} m_i X_i(t) \tag{14}$$

where $X_i(t)$ denotes the characteristic thermal patterns generated by the area represented by position i at time $t$with dimension N_x by N_y.

An important part of data reconstruction is to select the appropriate fixed frame interval. The suitable number of fixed frame intervals (N) depends on the correlation coefficients [44] between defect and nondefect areas. The smaller the value of the correlation coefficients, the better the separation result of PCA.

Fig. 3 illustrates the flow chart of the entire data processing operation, which contains 1) the preprocessing (noise reduction by substracting of the first frame), 2) selection of the appropriate fixed frame-interval by calculating the correlation coefficient and processing the OF, and 3) PCA processing. Fig. 4 shows the specific selection process of the fixed frame interval. The minIndex refers to the number of the most suitable interval.

Fig. 5 shows a schematic diagram of the detailed process of TPC. The input of PCA is generated by new image sequences after the processing of the OF between each two images with fixed frame intervals. The number of principal components of PCA is set as N_s. Finally, principal components are reconstructed as the spatial-transient patterns for crack detection.

E. Abstract Model

An abstract model is used to simulate a defect signal that behaves as a weak part and suffers from strong interference. This model enables a better interpretation of the TPC process. Fig. 6 demonstrates the schematic diagram of the abstract model. The induction coil is located at a certain distance (m) from the

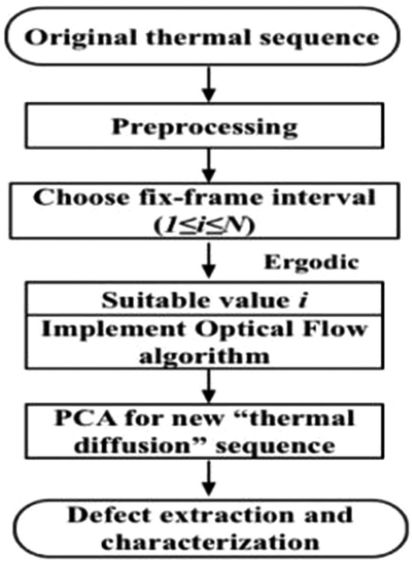

Fig. 3. Flow chart of the data processing of TPC.

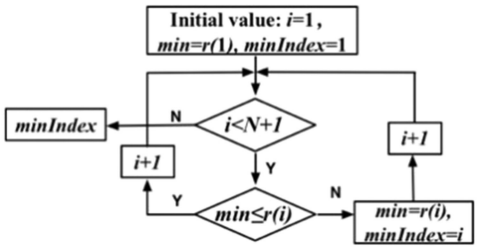

Fig. 4. Specific selection process of the optimum fixed frame-interval.

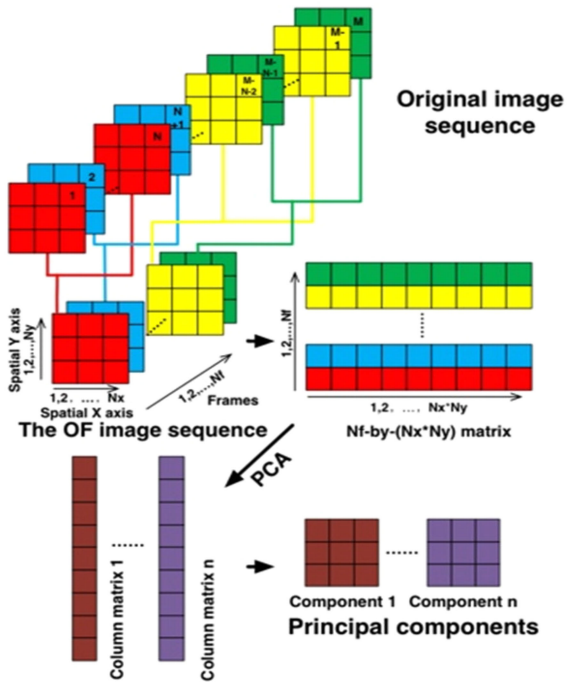

Fig. 5. Schematic diagram of TPC.

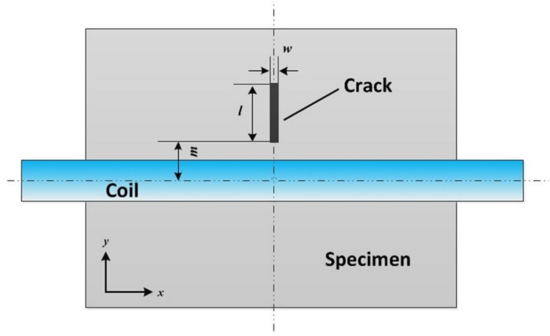

Fig. 6. Top view of the abstract model.

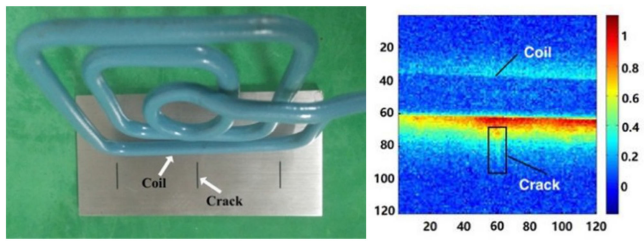

(a) (b)

Fig. 7. (a) Artificial crack with perpendicular crack under test. (b) Original transient temperature distribution at 5 ms.

crack that is perpendicular to the coil. The design purpose of the position between the coil and defects is to generate a weak defect signal in order to imitate the impact damage. This abstract model serves to illustrate the artificial crack sample as discussed in Fig. 7.

III. Results and Discussions

A. Experiment Setup

The Easyheat 224 from Cheltenham Induction Heating, Ltd., was used for induction heating, with a maximum excitation power of 2.4 kW, a maximum current of 400 A, and an excitation frequency range of 150–400 kHz. The excitation coil was made of 6.35-mm high-conductivity hollow copper tubing. The infrared system FLIR-A655sc was used to record the temperature change. It is a Stirling uncooled camera with a full frame 640 × 480 resolution of 7.5–14 μm InSb detectors. This camera has a sensitivity of <50 mK and a maximum full frame rate of 200 Hz. The temperature range is from −40 °C to 650 °C.

In the following sections, two case studies involving a perpendicular crack and fatigue natural cracks under impact damage are provided. In these experiments, the excitation frequency and current were set as 256 kHz and 380 A, respectively. The heating time was set as 0.2 s and the entire recording time was 4 s. Because the emissivity of the sample is unknown, a digital level (DL) is used to describe the temperature rather than Celsius degrees (°C). Specifically, the radiation of the object was sampled by using the commercial thermography software Altair in which the unit of radiation is DL. A nonlinear transfer function after calibration can convert the radiation (unit: DL)

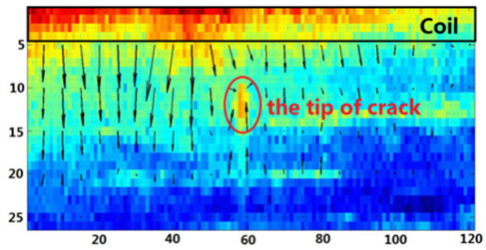

Fig. 8. Result of the optical flow algorithm for the artificial crack.

into temperature (unit: K/°C), which requires an operator setting several parameters such as emissivity background temperature, and transmission. In order to simplify the process, we used DL as a representation of temperature in the experiment.

B. Abstract Model-Artificial Crack in Steel Sample

The abstract model serves to simulate the valuable diagnosis information for the detection of a weak thermal signal. Fig. 7(a) demonstrates the abstract model, a steel sample with one perpendicular crack (*l:* 10 mm *w:* 0.3 mm *d:* 1 mm) constructed in the form of a rectangular block ($l \times w \times d$: 120 mm × 60 mm × 5 mm). During the experiment, both the coil and IR camera were placed above the defect side. The lift-off distance between the coil and sample was 1 mm. The distance (m) between the artificial crack and the excitation coil was equal to 3.5 mm.

Fig. 7(b) presents the results of the transient temperature distribution on the surface of the material at an early heating stage (5 ms) without any data processing. It shows that the area underneath the excitation coil has a higher temperature than the defect area. The reason is that the distribution of eddy current shows an exponential decay trend from the center of the straight wire to both flanks. The coil and artificial crack are positioned perpendicularly. This results in the hot spot appearing in the tip of the defect due to the diversion of eddy current when it encounters a discontinuity. Concurrently, it is revealed that the lateral thermal diffusion is seen to be feeble not only because of the great distance between the crack and coil, but also due to the parallel direction between the thermal diffusion and the defect. Even though the tip of the crack displays a weak hot spot, these thermal features are difficult to recognize due to the strong interference from the high temperature region under the coil.

The result of OF is shown in Fig. 8. The defect and nondefect areas present totally different thermal patterns. The arrows of OF converge around the defect, which indicate the disturbance of thermal behavior, hindered by the crack. In contrast, the direction of OF under the coil emerges as a horizontal translation, which is along the radial orientation of the coil and flows along with the temperature gradient. This result shows that the OF has the ability to extract the singular transient thermal behavior that enhances the detection of defect thermal patterns.

The correlation coefficients [29] are selected as the evaluation criteria to discover the adaptive fixed frame-interval to generate the new OF sequence. Unrelated variables will be divided into different components of PCA. Fig. 9 shows the correlation coefficient between the coil, the crack, and the sound area (means

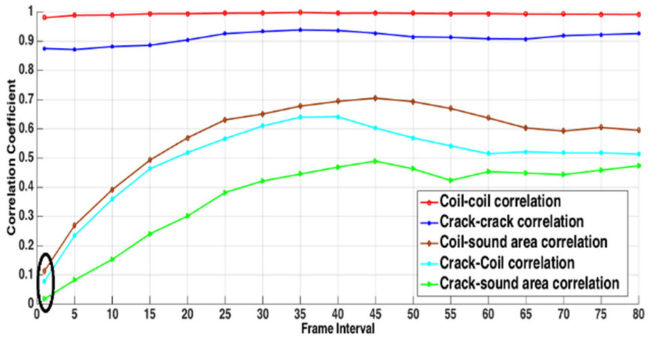

Fig. 9. Result of correlation coefficients for artificial crack.

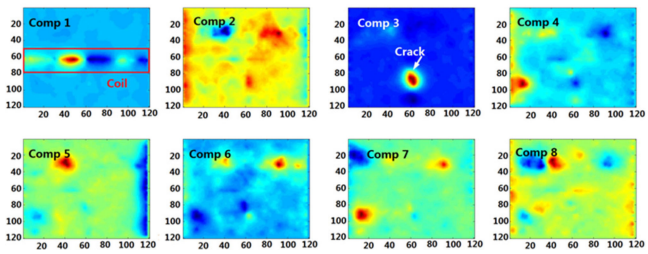

Fig. 10. Result of PCA after optical flow under steel sample testing.

non-defect area [24]). The traversal range of the frame interval is from 1 to 80. With the increase of the frame interval, the cross correlation coefficient of coil–coil and crack–crack remained at a high value.

This means that any region of the defect or coil could represent itself. Notwithstanding above, the correlation coefficient between the coil, the crack and the sound area presents an increasing trend with the rise of frame intervals. Thus, the small frame interval has the potential to fully separate the thermal informative patterns as marked in a black circle of Fig. 9. According to the results of the correlation coefficients, one fixed-frame interval is chosen for data reconstruction. Fig. 10 shows the PCA results where the number of principal components is set to eight. This number was given by a Monte-Carlo repeated experiment [45] involving 12 independent trials. The components one and two contain the coil information and the component three represents the tip information of the crack.

These results show that the TPC method has the potential to diagnose the microcrack under strong interference.

C. Natural Fatigue Cracks in Aircraft Brake Systems

A driven key, which has been removed from an aircraft in service with multicracks on the surface of the impact areas, is shown in Fig. 11(c). The impact areas with flaws are marked by red rectangles. As illustrated in Fig. 11(d), the driven key is fixed to bench vice and a pancake coil is used.

After the preprocessing, the one result of the OF algorithm between two thermal images is shown in Fig. 12. It presents the different thermal patterns between cracks and the sound area. The two white circle regions representing the thermal perturbation are defined as the suspected flaw areas (crack 1 and crack 2). The arrows of OF gather together around the defects,

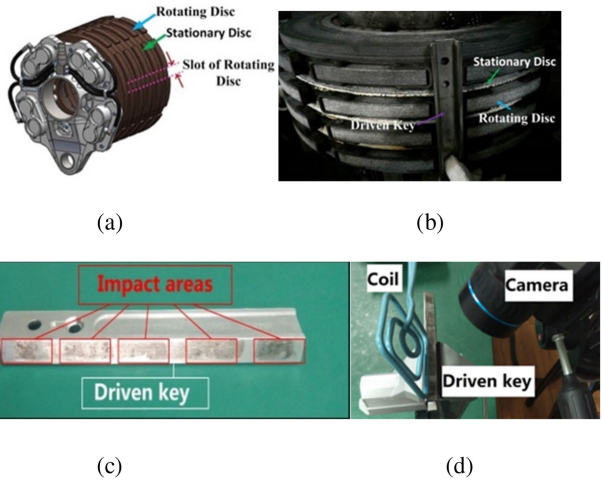

Fig. 11. (a) Schematic diagram of the braking system. (b) Real structure of the braking system. (c) Driven key sample with impact damage. (d) ECPT experiment setup.

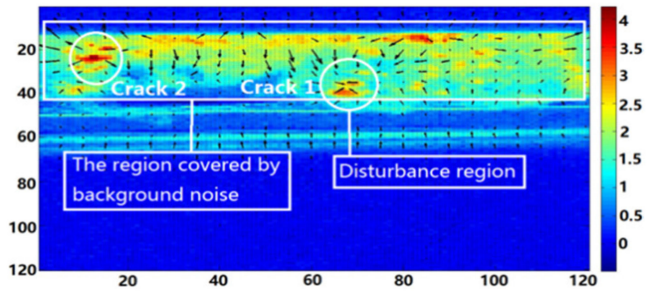

Fig. 12. Result of the optical flow algorithm for the natural cracks.

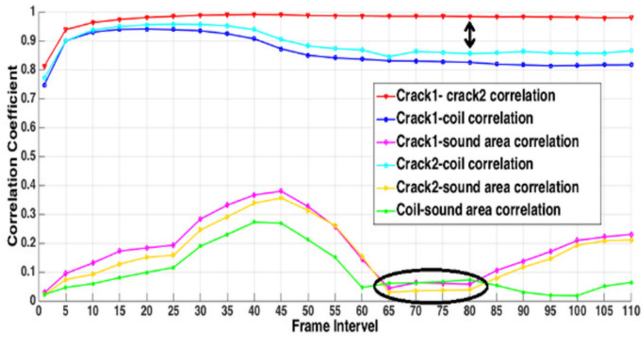

Fig. 13. Result of correlation coefficients for the natural cracks.

which indicate eddy current passing around the cracks and the disturbance of thermal behavior. In contrast, the direction of OF under the coil and the sound area without defect emerge as a horizontal translation. Fig. 13 shows the results of correlation coefficients for the natural crack detection. The regions of crack 1 and crack 2 are defined in Fig. 14. The results show that crack 1 and crack 2 maintain a high value of correlation coefficients regardless of the variation of the frame interval. Unfortunately, the correlation coefficients between the cracks and coil are also high. The reason is that the thermal pattern of the cracks is affected by the adjacent coil. To separate the thermal behavior of the crack and coil, a relatively small value

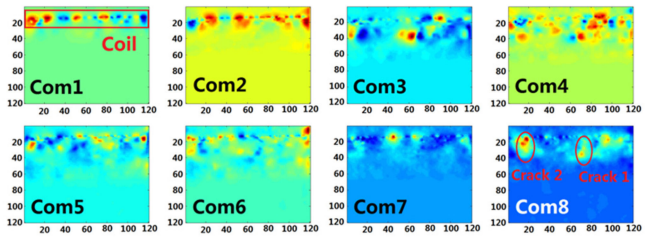

Fig. 14. Result of PCA after optical flow under impact damage.

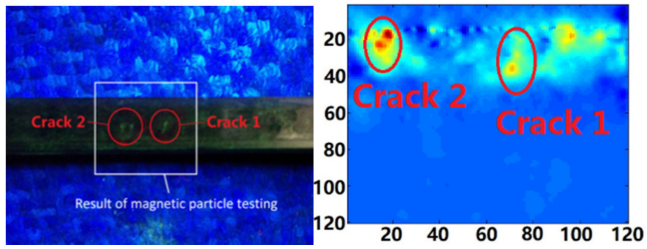

Fig. 15. Result comparison of MPT and the proposed method using ECPT: (a) magnetic particle testing; (b) TPC.

Fig. 16. Physical map of eight groups of specimen.

TABLE I
DEFINITION OF PRECISION AND RECALL

True positive (TP) A defect exists and is detected **False positive (FP)** No defect exists but one is identified	$\text{Precision} = \frac{\text{TP}}{\text{TP+FP}}$
False negative (FN) A defect exists but is not detected **True negative (TN)** No defect exists and none is detected	$\text{Recall} = \frac{\text{TP}}{\text{TP+FN}}$

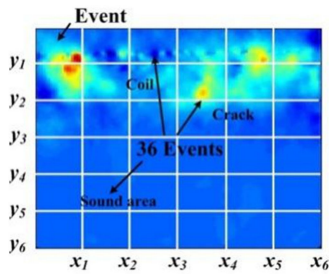

Fig. 17. Grid of the event segmentation for the F-score.

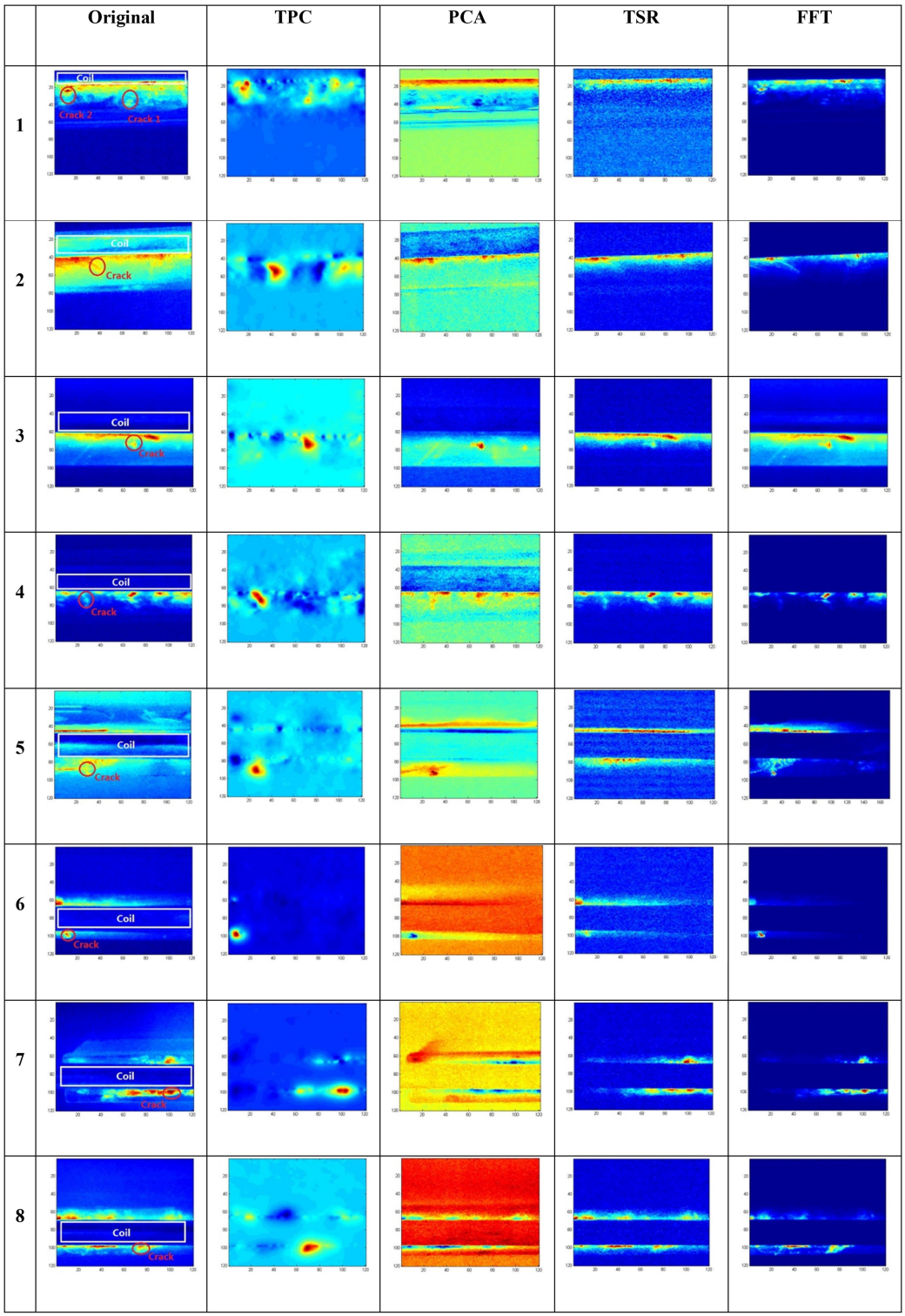

Fig. 18. Results of different signal processing method.

of correlation coefficients between the cracks and coil should be chosen so that the difference between the coil and the cracks could be as large as possible. As for the sound area, the value of correlation coefficients should be as small as possible. Therefore, the frame interval was chosen as the range [65, 80], which satisfies the above two conditions so that the value of correlation coefficients is at a minimum between the crack and coil & sound area. As an example, the 80 fixed-frame interval is demonstrated. The number of principal components of PCA is set to eight. In Fig. 14, the eighth principal component shows that the two fatigue cracks have been separated with minimal interference, and have been marked with red circles.

To validate the results, magnetic particle testing (MPT) is employed to serve as a validation NDT tool for the detection.

TABLE II
RESULTS OF THE QUANTITATIVE ANALYSIS

		1	2	3	4	5	6	7	8
TPC	F-SCORE(%)	85.7%	80.0	100.0%	100.0%	100.0%	100.0%	80.0	100.0%
	SNR(dB)	12.14	12.45	14.4	12.8	17.1	22.4	17.26	16.5
PCA	F-SCORE(%)	0.0	0.0	100.0%	0.0	33.3	100.0%	0.0	0.0
	SNR(dB)	✗	✗	11.2	✗	9.7	15.6	✗	✗
TSR	F-SCORE(%)	0.0	0.0	33.3	28.6	0.0	66.7	40.0	33.3
	SNR(dB)	✗	✗	2.7	−2.9	✗	11.2	13.10	8.2
FFT	F-SCORE(%)	50.0	66.7%	50.0	0.0	40.0	100.0%	40.0	33.3
	SNR(dB)	8.6	−0.8	3.8	✗	7.0	22.2	16.78	13.4

TABLE III
RESULTS OF F-SCORE DETAIL

		1	2	3	4	5	6	7	8
TPC	F-SCORE(%)	85.7	80.0	100.0	100.0	100.0	100.0	80.0	100.0
	TP	3	2	1	1	2	2	2	2
	FP	1	1	0	0	0	0	1	0
	FN	0	0	0	0	0	0	0	0
PCA	F-SCORE(%)	0.0	0.0	100.0	0	33.3	100.0	0.0	0.0
	TP	0	0	1	0	1	2	0	0
	FP	0	3	0	4	4	0	5	9
	FN	3	2	0	1	0	0	2	2
TSR	F-SCORE(%)	0.0	0.0	33.3	28.6	0.0	66.7	40.0	33.3
	TP	0	0	1	1	0	2	2	1
	FP	4	4	4	5	7	1	3	4
	FN	3	2	0	0	2	0	0	0
FFT	F-SCORE(%)	50.0	66.7	50.0	0.0	40.0	100.0	40.0	33.3
	TP	3	2	1	0	2	2	2	1
	FP	3	1	1	5	3	0	3	4
	FN	0	0	0	1	0	0	0	0

Fig. 15(a) illustrates the result of MPT. It validates that the flaws exist at the locations with fluorescence as well as two areas circled in Fig. 15(b). The comparison diagram shows that the results of the two methods coincide with each other. This result proves that TPC works equally well for natural cracks.

To verify the robustness of the proposed method, eight groups of different specimens have been validated. A detailed description of the eight groups composed of different specimens is given. All specimens are from the in-service aircraft braking system. Specimens are shown in Fig. 16 and all of them contain microcracks in the impact area. The material properties and structure of the eight specimens are the same. Take sample "A1" as an example in this paper, it is the most challenging case in which there exists two microcracks simultaneously. The MPT is employed as a standard NDT tool to generate the ground truth of the defects. The position and shape of all cracks in the specimens have been identified using MPT.

The comparison results between different detection approaches are shown in Table II and Table III. These methods include manual selection of original thermal imaging, TPC, PCA, TSR [21], [22], and Fourier analysis (FFT) [46]–[48]. In this case, the position of the coil and crack is known as prior information. Based on the results of Table II, a quantitative analysis is then provided by the events based F-score [49] and SNR [50] using the majority vote method [51].

The events based F-score [49] is defined as follows:

$$F = \frac{(\alpha^2 + 1) \times \text{Precision} \times \text{Recall}}{(\alpha^2 \times \text{Precision}) + \text{Recall}}. \tag{15}$$

The Precision and Recall is described in Table I. α in (15) is a default value that determines the weight of the Precision and Recall. In this paper, the value of α is set to 1 which means that the Recall is as important as the Precision. In Fig. 17, all of the results of Fig. 18 will be divided into 6×6 square grids. According to the results of MPT, each region as an event could be determined by the attribute (defect or nondefect) for the calculation of the F-score.

The SNR [50] then further evaluates the thermal contrast between the defective and nondefective region. The calculation of SNR (dB) is defined in the equation below:

$$\begin{aligned} \text{SNR} &= \frac{S}{N} \\ &= 20\log_{10}\left(\frac{\text{abs}(S\text{area}_{\text{Average}} - N\text{area}_{\text{Average}})}{\sigma(N\text{area}_{\text{Average}})}\right)[\text{dB}] \end{aligned} \tag{16}$$

where $S\text{area}_{\text{Average}}$ and $(N\text{area}_{\text{Average}})$ are the average temperature in the defect and nondefect regions (the entire image except the defect area), respectively. $\sigma(\text{Narea}_{\text{Average}})$ is the temperature standard deviation in the nondefective region.

The quantitative analysis involving the event-based F-score and SNR is presented in Table II and Table III. The "✗" in SNR results refers to an occurrence in which the method could not detect the microcrack in the corresponding experiment. In the tests 1 and 2, the F-score and SNR of TPC are equal to 85.7% and 80.0%, with the SNR of 12.1 and 12.5 dB, respectively. Compared with FFT, the F-score improves by 35.7% and 13.3% and the SNR is enhanced with 3.6 and 13.2 dB, respectively. Nevertheless, the methods of PCA and TSR do not perform a good detection of the microimpact crack. From test 3 to 5, the results obtained using TPC have obvious superiority. The F-score of TPC is equivalent to 100.0% that indicates that the microimpact crack is successfully detected. In contrast, other methods have an unsatisfactory performance that still contains the complex background as well as noise information. Meanwhile, compared with the SNR of the remaining methods, the SNR of TPC leads to an improvement of 3.2, 9.9, and 7.5 dB for PCA, 11.7 and 15.7 dB for TSR, and finally, 10.7 and 10.0 dB for FFT. In test 6, all of the above methods basically detected the defect and four signal processing methods have a similar quality behavior. In test 7 and 8, the PCA process could not distinguish the crack location. The F-score and SNR of TPC are equivalent to 80.0%, 100.0% and 17.3 and 16.5 dB, respectively. Compared with TSR and FFT, the F-score of TPC improves 40% and 66.7%, respectively. The SNR of TPC is enhanced by 4.1 and 0.5 dB for TSR and 8.3 and 3.1 dB for FFT, respectively.

From the overall analysis, the average of the F-score and SNR of TPC is 93.2% and 15.6 dB. Compared with PCA, TSR and FFT, the average of the TPC F-score improves 59.9%, 67.67%, and 45.7% and SNR improves by 10.7, 11.6, and 6.7 dB, respectively. In general, compared to these classical algorithms, the TPC method enhances the extraction of the weak singular thermal spatial-transient pattern and compensates effectively to strengthen the detectability of microcracks.

IV. Conclusion

This paper proposes a method termed as the TPC to extract and separate thermal spatial-transient patterns in order to diagnose microcracks. The data processed from the proposed method have been elaborated and analyzed. The data reconstruction has been presented by the successive OF between every two images with a fixed frame-interval in turn calculation. The most suitable number of fixed frame-interval depends on the correlation coefficients. Further mining of the spatial-transient patterns to separate the faulty areas and to enhance the detection sensitivity has been undertaken by PCA. The obtained experimental results have strongly validated the effectiveness and robustness of the proposed method by the abstract model and natural cracks on the impact damage area of the driven key. These quantitative analysis results have shown that the proposed method is a viable candidate as an alternative method to the MPT that is currently used in industry.

The proposed method has also shed new light not only on the deeper utilization of physical mechanisms of inductive heating propagation, but also on better modeling and mining of the kinematic spatial-transient thermal patterns in quantitative defect detection. Future work will focus on the robustness and universality testing of the proposed method on more specimens and different thermal platforms.

References

[1] V. Vavilov, "Thermal NDT: Historical milestones, state-of-the-art and trends," *Quant. Infrared Thermogr. J.*, vol. 11, no. 1, pp. 66–83, 2014.

[2] R. Yang and Y. He, "Optically and non-optically excited thermography for composites: A review," *Infrared Phys. Technol.*, vol. 75, pp. 26–50, 2016.

[3] S. Bagavathiappan *et al.*, "Infrared thermography for condition monitoring—A review," *Infrared Phys. Technol.*, vol. 60, no. 5, pp. 35–55, 2013.

[4] L. J. Bond, "Through the looking glass: The future for NDE?[C]," in *Proc. 40th Annu. Rev. Progress Quantitative Nondestructive Evaluation*, vol. 1581, no. 1, 2014, pp. 21–35.

[5] H. Zhang *et al.*, "Optical and mechanical excitation thermography for impact response in basalt-carbon hybrid fiber-reinforced composite laminates," *IEEE Trans. Ind. Informat.*, vol. 14, no. 2, pp. 514–522, Feb. 2018.

[6] G. H. DeVlieg, "System and method for aircraft braking system usage monitoring," U.S. Patent 6 659 233, Dec. 12, 2003.

[7] C. T. O'Connell and H. Oyama, "Aircraft brake system," U.S. Patent 9 108 726, Aug. 18, 2015.

[8] M. Kroes, J. Rardon, and M. Nolan, *Aircraft Basic Science[M]*, 7th ed., McGraw Hill Professional, 2013.

[9] *Standard Reference Radiographs for Investment Steel Castings of Aerospace Applications*, ASTM, West Conshohocken, ASTM Standard E192, 1999

[10] M. D. Sangid, "The physics of fatigue crack initiation," *Int. J. Fatigue*, vol. 57, pp. 58–72, 2013.

[11] B. Gao, W. L. Woo, Y. He, and G. Y. Tian, "Unsupervised sparse pattern diagnostic of defects with inductive thermography imaging system," *IEEE Trans. Ind. Informat.*, vol. 12, no. 1, pp. 371–383, Feb. 2015.

[12] Y. He and R. Yang, "Eddy current volume heating thermography and phase analysis for imaging characterization of interface delamination in CFRP," *IEEE Trans. Ind. Informat.*, vol. 11, no. 6, pp. 1287–1297, Dec. 2015.

[13] V. P. Vavilov and D. D. Burleigh, "Review of pulsed thermal NDT: Physical principles, theory and data processing," *Ndt E Int.*, vol. 73, no. 1, pp. 28–52, 2015.

[14] B. Gao, Y. He, W. L. Woo, G. Y. Tian, J. Liu, and Y. Hu, "Multidimensional tensor-based inductive thermography with multiple physical fields for offshore wind turbine gear inspection," *IEEE Trans. Ind. Electron.*, vol. 63, no. 10, pp. 6305–6315, Oct. 2016.

[15] J. León, X. Perpiñà, J. Sacristán, M. Vellvehi, A. Baldi, and X. Jordà, "Functional and consumption analysis of integrated circuits supplied by inductive power transfer by powering modulation and lock-in infrared imaging," *IEEE Trans. Ind. Electron.*, vol. 62, no. 12, pp. 7774–7785, Dec. 2015.

[16] S. Yin, X. Li, H. Gao, and O. Kaynak, "Data-based techniques focused on modern industry: An overview," *IEEE Trans. Ind. Electron.*, vol. 62, no. 1, pp. 657–667, Jan. 2014.

[17] O. Lucia, P. Maussion, E. J. Dede, and J. M. Burdio, "Induction heating technology and its applications: Past developments, current technology, and future challenges," *IEEE Trans. Ind. Electron.*, vol. 61, no. 5, pp. 2509–2520, May 2014.

[18] O. Lucia, P. Maussion, E. J. Dede, and J. M. Burdio, "Introduction to the special section on induction heating systems," *IEEE Trans. Ind. Electron.*, vol. 61, no. 5, pp. 2504–2508, May 2014.

[19] H. Zhang *et al.*, "Enhanced infrared image processing for impacted carbon/glass fiber-reinforced composite evaluation," *Sensors*, vol. 18, no. 1, 2017, Art. no. 45.

[20] C. Ibarra-Castanedo, J. R. Tarpani, and X. P. V. Maldague, "Nondestructive testing with thermography," *Eur. J. Phys.*, vol. 34, no. 6, 2013, Art. no. S91.

[21] S. M. Shepard, "Advances in pulse thermography," *Proc. SPIE*, vol. 4360, pp. 511–515, 2001.

[22] S. M. Shepard and J. R. Lhota, "Reconstruction and enhancement of active thermographic image sequences," *Opt. Eng.*, vol. 42, no. 5, pp. 1337–1342, 2003.
[23] B. Gao, L. Bai, W. L. Woo, G. Y. Tian, and Y. Cheng, "Automatic defect identification of eddy current pulsed thermography using single channel blind source separation," *IEEE Trans. Instrum. Meas.*, vol. 63, no. 4, pp. 913–922, Apr. 2014.
[24] X. Maldague and S. Marinetti, "Pulse phase infrared thermography," *J. Appl. Phys.*, vol. 79, no. 5, pp. 2694–8, 1996.
[25] C. Ibarra-Castanedo, D. González, M. Klein, M. Pilla, S. Vallerand, and X. Maldague, "Infrared image processing and data analysis," *Infrared Phys. Technol.*, vol. 46, no. 2, pp. 75–83, 2004.
[26] K. Chatterjee and S. Tuli, "Image enhancement in transient lock-in thermography through time series reconstruction and spatial slope correction," *IEEE Trans. Instrum. Meas.*, vol. 61, no. 4, pp. 1079–1089, Apr. 2012.
[27] J. Vrana *et al.*, "Mechanisms and models for crack detection with induction thermography," *Amer. Inst. Phys.*, vol. 975, no. 1, pp. 475–482, 2008.
[28] S. Dudzik, "Analysis of the accuracy of a neural algorithm for defect depth estimation using PCA processing from active thermography data," *Infrared Phys. Technol.*, vol. 56, no. 36, pp. 1–7, 2013.
[29] J. Peng *et al.*, "Investigation into eddy current pulsed thermography for rolling contact fatigue detection and characterization," *Ndt E Int.*, vol. 74, no. 6, pp. 72–80, 2015.
[30] B. Gao *et al.*, "Quantitative validation of Eddy current stimulated thermal features on surface crack," *Ndt E Int.*, vol. 85, pp. 1–12, 2017.
[31] Y. Wang *et al.*, "Diffusion and separation mechanism of transient electromagnetic and thermal fields," *Int. J. Thermal Sci.*, vol. 102, pp. 308–318, 2016.
[32] B. Gao, L. Bai, W. L. Woo, and G. Tian, "Thermography pattern analysis and separation," *Appl. Phys. Lett.*, vol. 104, no. 25, 2014, Art. no. 251902.
[33] B. Gao, W. L. Woo, and G. Y. Tian, Electromagnetic thermography nondestructive evaluation: Physics-based modeling and pattern mining," *Sci. Rep.* vol. 25480, no. 6, 2016.
[34] L. Cheng and G. Y. Tian, "Transient thermal behavior of eddy-current pulsed thermography for nondestructive evaluation of composites," *IEEE Trans. Instrum. Meas.*, vol. 62, no. 5, pp. 1215–1222, May 2013.
[35] N. P. Avdelidis and D. P. Almond, "Transient thermography as a through skin imaging technique for aircraft assembly: modelling and experimental results," *Infrared Phys. Technol.*, vol. 45, no. 2, pp. 103–114, 2004.
[36] L. Bai, S. Tian, Y. Cheng, G. Y. Tian, Y. Chen, and K. Chen, "Reducing the effect of surface emissivity variation in eddy current pulsed thermography," *IEEE Sens. J.*, vol. 14, no. 4, pp. 1137–1142, Apr. 2014.
[37] M. Kasemann, B. Walter, C. Meinhardt, J. Ebser, W. Kwapil, and W. Warta, "Emissivity-corrected power loss calibration for lock-in thermography measurements on silicon solar cells," *J. Appl. Phys.*, vol. 103, no. 11, 2008, Art. no. 113503.
[38] T. Schmugge, A. French, J. C. Ritchie, A. Rango, and H. Pelgrum, "Temperature and emissivity separation from multispectral thermal infrared observations," *Remote Sens. Environ.*, vol. 79, no. 2, pp. 189–198, 2002.
[39] R. Yang, Y. He, B. Gao, and G. Y. Tian, "Inductive pulsed phase thermography for reducing or enlarging the effect of surface emissivity variation," *Appl. Phys. Lett.*, vol. 105, no. 18, 2014, Art. no. 184103.
[40] B. Gao, L. Bai, W. L. Woo, and G. Tian, "Thermography pattern analysis and separation," *Appl. Phys. Lett.*, vol. 104, no. 25, 2014, Art. no. 251902.
[41] Y. Gao and G. Y. Tian, "Emissivity correction using spectrum correlation of infrared and visible images," *Sens. Actuators A: Phys.*, vol. 270, pp. 8–17, 2018.
[42] B. K. P. Horn and B. G. Schunck, "Determining optical flow," *Artif. Intell.*, vol. 17, pp. 185–203, 1981.
[43] G. J. Jang and T. W. Lee, "A maximum likelihood approach to single-channel source separation," *J. Mach. Learn. Res.*, vol. 4, pp. 1365–1392, 2003.
[44] J. Lee Rodgers and W. A. Nicewander, "Thirteen ways to look at the correlation coefficient," *Amer. Statistician*, vol. 42, no. 1, pp. 59–66, 1988.
[45] J. P. C. Kleijnen, "Design and analysis of Monte Carlo experiments[M]," in *Handbook of Computational Statistics*. Berlin, Heidelberg, Germany: Springer, 2012, pp. 529–547.
[46] Y. He *et al.*, "Eddy current pulsed phase thermography for subsurface defect quantitatively evaluation[J]," *Appl. Phys. Lett.*, vol. 103, no. 14, 2013, Art. no. 144108.
[47] H. Yang *et al.*, "Transient-spatial pattern mining of eddy current pulsed thermography using wavelet transform," *Chin. J. Mech. Eng.*, vol. 27, no. 4, pp. 768–778, 2014.
[48] T. Liang *et al.*, "Low energy impact damage detection in CFRP using eddy current pulsed thermography," *Composite Struct.*, vol. 143, pp. 352–361, 2016.
[49] D. M. Powers, "Evaluation: From precision, recall and F-measure to ROC, informedness, markedness and correlation," *J. Mach. Learn. Technol.*, vol. 2, no. 1, pp. 37–63, 2011.
[50] M. A. Omar and Y. Zhou, "A quantitative review of three flash thermography processing routines," *Infrared Phys. Technol.*, vol. 51, no. 4, pp. 300–306, 2008.
[51] P. L. Krapivsky, S. Redner, and E. Ben-Naim, *A Kinetic View of Statistical Physics*. Cambridge, U.K.: Cambridge Univ. Press, 2010, pp. 831–832.

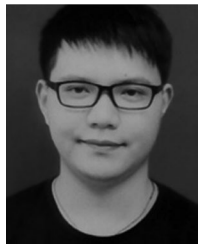

Yizhe Wang (S'18) received the B.Sc. degree in physics from Shenyang Normal University, Shenyang, China, in 2012, and the M.E. degree in instrument science and technology from the University of Electronic Science and Technology of China (UESTC), Chengdu, China, in 2014. He is currently working toward the Ph.D. degree in quantitative fatigue assessment and health state monitoring using infrared thermography at UESTC and Laval University, Quebec, Canada.

His current research interests include sensor design, fatigue damage, quantitative nondestructive testing and evaluation, sensor signal processing, and machine learning.

Bin Gao (M'12–SM'14) received the B.Sc. degree in communications and signal processing from Southwest Jiao Tong University, China, in 2005, the M.Sc. degree (with distinction) in communications and signal processing, and the Ph.D. degree from Newcastle University, Newcastle upon Tyne, U.K., in 2007 and 2011, respectively.

From 2011 to 2013, he was a Research Associate with the same university on wearable acoustic sensor technology. Currently, he is a Professor with the School of Automation Engineering, University of Electronic Science and Technology of China (UESTC), Chengdu, China. He has coordinated several research projects from the National Natural Science Foundation of China. His research interests include sensor signal processing, machine learning, social signal processing, nondestructive testing, and evaluation where he actively publishes in these areas. He has authored or coauthored more than 60 papers on these topics on various journals and international conference proceedings.

Wai Lok Woo (M'09–SM'11) was born in Malaysia. He received the B.Eng. degree (1st Class Hons.) in electrical and electronics engineering and the Ph.D. degree from the Newcastle University, Newcastle upon Tyne, U.K, in 1993 and 1998, respectively.

He is currently a Senior Lecturer and the Director of Operations with the School of Electrical and Electronic Engineering, Newcastle University. His major research interests include the mathematical theory and algorithms for nonlinear signal and image processing. This also includes the areas of machine learning for signal processing, blind source separation, multidimensional signal processing, signal/image deconvolution and restoration. He has an extensive portfolio of relevant research supported by a variety of funding agencies. He has authored and coauthored more than 250 papers on these topics on various journals and international conference proceedings. He is currently an Associate Editor of several international journals and has served as the Lead Editor of journals' special issues.

Dr. Woo was awarded the IEE Prize and the British Scholarship to continue his research work.

Gui Yun Tian (M'01–SM'03) received the B.Sc. degree in metrology and instrumentation and the M.Sc. degree in precision engineering both from the University of Sichuan, Chengdu, China, in 1985 and 1988, respectively, and the Ph.D. degree from the University of Derby, Derby, U.K., in 1998.

From 2000 to 2006, he was a Lecturer, Senior Lecturer, Reader, Professor, and the Head of the group of Systems Engineering, respectively, with the University of Huddersfield, U.K. Since 2007, he has been based at Newcastle University, Newcastle upon Tyne, U.K., where he has been a Chair Professor in sensor technologies. Currently, he is also an Adjunct Professor with the School of Automation Engineering, University of Electronic Science and Technology of China, Chengdu. He has coordinated several research projects from the Engineering and Physical Sciences Research Council, Royal Academy of Engineering and FP7, on top of this he also has good collaboration with leading industrial companies such as Airbus, Rolls Royce, BP, nPower, Networkrail, and TWI.

Xavier Maldague (SM'02) received the B.Sc. degree in electrical engineering and M.Sc. degree in tridimensional image acquisition from the Université Laval, Quebec City, Canada, in 1982 and 1984, respectively, and the Ph.D. degree from the Université Laval, Quebec City, Canada, in 1989.

He was the Head of the Department of Electrical and Computing Engineering, Université Laval, Québec City, Canada (from 2003 to 2008), where he has been a Full Professor (since 1989). He has trained more than 50 graduate students (M.Sc. and Ph.D.) and has more than 300 publications. His research interests include infrared thermography, nondestructive evaluation techniques and vision/digital systems for industrial inspection. He holds a Tier 1 Canada Research Chair in infrared vision.

Prof. Maldague chairs the Quantitative Infrared Thermography Council. He is a Fellow of the Canada Engineering Institute, an Honorary Fellow of the Indian Society of Nondestructive Testing, and a Fellow of the Alexander von Humbolt Foundation in Germany. Within IEEE Canada, he was Co-Editor of the IEEE CANADIAN JOURNAL OF ELECTRICAL AND COMPUTER ENGINEERING from 2003 to 2007. From 2002 to 2004 and from 2015 to 2017, he chaired the IEEE Quebec City Section. In 2004, he was awarded the IEEE J. J. Archambault Award for his dedication to IEEE and his contributions to engineering progress. From 2008 to 2011, he was the IEEE Canada Publications and Communications Group Chair.

Li Zheng is currently working toward the B.Sc. degree in the UESTC UoG Joint School, University of Electronic Science and Technology of China, Chengdu, China.

Her research interests include nondestructive testing and image processing.

Zheyou Guo is currently working toward the B.Sc. degree in the UESTC UoG Joint school, University of Electronic Science and Technology of China, Chengdu, China.

Her research interests include nondestructive testing and deep learning.

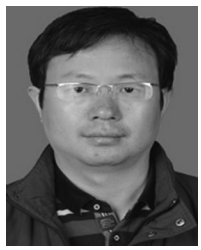

Yuyu Zhu received the B.Sc. degree in automation and the M.Sc. degree in control theory and engineering from the Southwest University of Science and Technology, in 2002 and 2009, respectively. He is currently working toward the Ph.D. degree with the University of Electronic Science and Technology of China, Chengdu, China.

He is an Associate Professor with the School on Monitoring and Control Technology and Power Electronics Technology, University of Electronic Science and Technology of China. His research interests include nondestructive testing and evaluation, power electronics technology.